Aerosol and Air Quality Research, 15: 945–957, 2015

ISSN: 1680-8584 print / 2071-1409 online
doi: 10.4209/aaqr.2014.05.0099

Aerosol Column Size Distribution and Water Uptake Observed during a Major Haze Outbreak over Beijing on January 2013

Ying Zhang[1], Zhengqiang Li[1*], Juan Cuesta[2], Donghui Li[1], Peng Wei[1], Yisong Xie[1], Lei Li[1]

[1] *State Environmental Protection Key Laboratory of Satellite Remote Sensing, Institute of Remote Sensing and Digital Earth, Chinese Academy of Sciences, PO Box 100101, Beijing, China*
[2] *Laboratoire Inter-Universitaire des Systèmes Atmosphériques, Université Paris Est Créteil, PO Box 94010, Créteil Cedex, France*

ABSTRACT

Haze can cause serious atmospheric pollution affecting air quality, human health and even global climate. In order to investigate aerosol columnar size distribution and water uptake during haze evolution, we analyse ground-based observations during an extreme winter pollution case at Beijing on 12 January 2013 (haze day) as compared to those registered on 9 January (non-haze day). We study the evolution of the aerosol size distribution using retrievals from a ground-based CIMEL sun-sky radiometer of the Aerosol Robotic Network (AERONET). Our results show that while the hourly volume growth rate of a sub-micron fine mode presented in the size distribution remains below 0.010 $\mu m^3/\mu m^2$/hr during the non-haze day, it can rapidly increase during haze pollution event, reaching a maximum value of 0.075 $\mu m^3/\mu m^2$/hr. The mean size of fine mode particles becomes larger during the pollution event, while it is reduced for coarse mode particles. The mean volume of water uptake is 0.013 $\mu m^3/\mu m^2$ in haze day, being about 13 times larger than that in non-haze day. Meanwhile, the volume of water-soluble inorganic aerosols increases from 0.036 to 0.298 $\mu m^3/\mu m^2$, partly explained by the increase of water uptake during the haze event and also likely by accumulation of particle matters due to stagnating atmospheric conditions. The increase of water-soluble particle volume, which is enhanced by water uptake, significantly contributes to haze evolution.

Keywords: Aerosol size distribution; Water uptake; Haze; Remote sensing; Beijing.

INTRODUCTION

Haze is an important air pollution phenomenon that leads to visibility below 10 km for relative humidity (RH) less than about 90% (Wu *et al.*, 2006). Haze formation is mainly due to atmospheric suspended fine particles, derived from anthropogenic emissions including industrials, vehicles, and secondary aerosol formations, which scatter and absorb the incident sunlight (Liu *et al.*, 2013). In the past three decades, the emission of aerosols and precursors into the atmosphere has greatly increased, leading to visibilities reduction, air quality deterioration, and negative influence on human health (Dockery and Pope, 1994; Pope *et al.*, 2002; Künzli *et al.*, 2005; Brook *et al.*, 2010). Meanwhile, perturbation to the atmospheric radiation field from the increase of aerosols loading could contribute to global climate changes (IPCC, 2013).

Haze has been extensively studied (Chen *et al.*, 2003; Wu *et al.*, 2005; Sun *et al.*, 2006; Wu *et al.*, 2006; Du *et al.*, 2011; Kang *et al.*, 2013a; Kang *et al.*, 2013b; Li *et al.*, 2013; Liu *et al.*, 2013; Sun *et al.*, 2013) focusing on the formation and evolution mechanism, aerosol microphysical and chemical properties. A good relationship is found at Beijing between haze pollution and meteorological factors, such as the planetary boundary layer height (PBLH), RH and atmospheric vertical stratification leading to enhanced stability (Liu *et al.*, 2013). In general, particles are accumulated near the surface when the PBLH decreases or remains stable, and they are enlarged by water uptake, which leads to the increase of the volume of the aerosols, thus strengthening sunlight attenuation and decreasing visibility (Chu *et al.*, 2013; Tan *et al.*, 2013; Zieger *et al.*, 2014). Also, haze pollution is reinforced by sustained emission of particles and precursors emitted by anthropogenic sources (Wu *et al.*, 2005; Sun *et al.*, 2006; Wang *et al.*, 2006; Du *et al.*, 2011). In North China, regional haze pollution happens frequently especially during winter and spring seasons because of both the enhanced heating/traffic/industrial emissions and the stable meteorological conditions (Sun *et al.*, 2006; Wang *et al.*, 2006). Moreover, some researcheres studied the variations in

* Corresponding author.
Tel.: +86 10 64857437; Fax: +86 10 6480 6225
E-mail address: lizq@radi.ac.cn

aerosol microphysical and chemical properties during haze pollution (Sun *et al.*, 2006; Wang *et al.*, 2006; Cheng *et al.*, 2006, 2008a, b; Liu *et al.*, 2008; Sun *et al.*, 2013). Sun *et al.* (2013) find that water-soluble aerosols are the most of particle matters during haze pollution events, while being mostly marked by fine particles. Water-soluble aerosols are directly affected by water vapour, which induces a significant hygroscopic growth (Liu *et al.*, 2008).

At present, quantitative analyses of aerosol compositions are usually obtained from filter sampling approaches. Aerosol compositions derived from in situ sampling are mainly daily average values. However, the microphysical properties of aerosols can vary significantly during formation and transport. It is still difficult to capture quick variations of aerosol composition using the filter sampling method. Aerosols can also be observed in the ambient environment by remote sensing approach, without heating or sampling. Advanced inversion techniques have been developed and applied to ground-based radiometric measurements for the retrieval of aerosol optical and microphysical properties (Nakajima *et al.*, 1983, 1996; Dubovik *et al*., 2000; Li *et al.*, 2006). Based on these aerosol optical properties, Schuster *et al.* (2005) derived the particle composition by quantifying the fraction of water, water-soluble and black carbon. They also quantified the importance of aerosol water uptake (Schuster *et al.*, 2009). Li *et al.* (2013a) and Wang *et al.* (2013) further improved the three-element composition method by adding mineral dust and brown carbon as additional elements, in order to investigate the properties of aerosol mixtures in Beijing.

In this study, we focus on the relationship between water-soluble aerosol, water content, and total aerosol volume concentration during a haze pollution event based on ground-based remote sensing measurements. In order to examine the evolution of aerosol size growth and composition, the aerosol hourly growth ratio and size parameters are calculated from volume size distributions and aerosol composition is retrieved from complex refractive indexes, obtained from AERONET sun-sky radiometer inversions. The data and methods are described in section 2. We examine the variation of aerosol properties related to RH during the haze day with respect to that of the non-haze day in section 3. The discussions and conclusions are presented in section 4.

DATA AND METHODS

Data Collection

In this study, we obtain the Aerosol Optical Depth (AOD) and aerosol optical/microphysical retrieval data (Level 1.5) of atmospheric column over Beijing site from AERONET website (http://aeronet.gsfc.nasa.gov). $PM_{2.5}$ (particulate matters with aerodynamic diameter less than 2.5 μm) mass concentrations are observed by a MetOne BAM 1020 instrument at U.S. Embassy at Beijing (Zhang and Li, 2013). Meteorological observations including temperature, RH and wind speed every 5 minutes are provided by World Meteorological Organization (WMO) weather station (No. 54511) at Beijing. Hourly $PM_{2.5}$ (in $\mu g/m^3$), AOD and other meteorological measurements, such as RH and wind speed, are then used to identify the peak of haze pollution and evaluate the particle growth in term of mass concentration.

In January 2013, there were five heavily polluted periods caused by haze over the Beijing area (Li *et al.*, 2013b), among which the second one (10–14 January 2013) was the most serious. We calculate the aerosol properties in January 2013, and collect data on 9 and 12 January to study the effects of RH on haze pollution. We consider that on 9 January relatively clean atmospheric conditions prevailed, while on 12 January a heavy pollution event occurred, with $PM_{2.5}$ concentrations larger than 500 $\mu g/m^3$ and AOD (440 nm) larger than 1.5. Meanwhile, most surface measurements show a RH higher than 80% on 12 January and relatively dry conditions (lower than 40%) on 9 January. In addition, no rain or snow occurred between these two days over the regions, with consequently no aerosol scavenging during this period. In order to obtain the transport pathway of air parcels that passed through Beijing, a 48-h backward trajectory analysis by Hybrid Single Particle Lagrangian Integrated Trajectory (HYSPLIT) model was carried out at heights of 10, 500, 1000 and 2000 meters above ground level on 9 January (ending at 9:00, 11:00, 13:00 and 15:00 local time) and 12 January (ending at 10:00, 11:00, 12:00 and 13:00), respectively. We also obtain the black carbon (BC) mass concentration near the ground using a co-located aethalometer (Magee Scientific AE51) instrument in order to compare with sun-sky radiometer retrievals in January 2013.

Method

Aerosol Volume Hourly Growth Ratio

The changes in aerosol volume can be attributed to the effects of aerosol activation, hygroscopic growth, coagulation and chemical reactions, etc. In order to study the changes in aerosol volume with time, we obtain the hourly variations in aerosol volumes by calculating the hourly growth ratio (HGR) as follows:

$$\mathrm{HGR}(r, t) = \left[\frac{dV}{d\ln r}(r, t2) - \frac{dV}{d\ln r}(r, t1)\right] \Big/ (t2 - t1), \qquad (1)$$

where, $dV/d\ln r(r, t)$ is aerosol volume size distribution at time t (local time, hereafter); t1 and t2 are the observation times. Indeed, the HGR is a difference of aerosol volume size distributions in the unit time. As for the AERONET-derived size distribution dV/dlnr, HGR is given for each particle radius r.

Size Distribution Breaking Down

In this study, we break down the dV/dlnr size distribution, given in volume concentration for each radius r by the AERONET retrieval, into Log-Normal Modes (LNM) following the method developed by Cuesta *et al.*, (2008). Each LNM is then described by 3 parameters: the modal concentration C_i, modal radius r_i and geometric standard deviation σ_i. In order to obtain these parameters, a kernel function of root mean square differences of the volume distributions (the calculated one with LNMs vs. the measured one by AERONET) is minimized iteratively using the Nelder-Mead simplex algorithm (Cuesta *et al.*, 2008). We choose multi-modal lognormal distributions to fit the AERONET

retrieved aerosol size distributions by the following formula:

$$\frac{dV}{dlnr}(r) = \sum_{i=1,n} \frac{C_i}{\sqrt{2\pi}\left|ln\sigma_i\right|} \exp\left[-\frac{1}{2}\left(\frac{lnr - lnr_i}{ln\sigma_i}\right)^2\right], \quad (2)$$

where dV/dlnr(r) (in unit of $\mu m^3/\mu m^2$) is the volume size distribution, C_i ($\mu m^3/\mu m^2$) and r_i (μm) and σ_i are the volume modal concentration, median radius and its standard deviation of each LNM mode, respectively. In most cases of this study, bimodal distributions with a fine ($0.05\ \mu m \le r \le 1\ \mu m$) and a coarse ($1\ \mu m < r \le 15\ \mu m$) modes are used, except for one case where (see section 3.2) a tri-modal distribution is considered (with a "Quasi-Conservative" Fine (QCF) mode of $0.05\ \mu m \le r \le 0.15\ \mu m$ and a "Variable" Fine (VF) mode of $0.15\ \mu m < r \le 1\ \mu m$).

Aerosol Water Uptake

Schuster *et al.* (2005) developed an algorithm to derive the aerosol composition using the mixture complex refractive indexes, based on the ground-based remote sensing measurements. Arola *et al.* (2011), Wang *et al.* (2013) and Li *et al.* (2013a) further developed the algorithm. This algorithm is employed here, where water uptake is regarded as a parent material with refractive index of 1.337346-0.0i, 1.332382-0.0i, 1.329633-0.0i and 1.328053-0.0i at 440 nm, 675 nm, 870 nm and 1020 nm wavelengths, respectively, black carbon as soot (1.95-0.79i at the four wavelengths), sulfates, nitrates and ammoniums as water-soluble substance (note that "water-soluble" aerosol in this paper refers to water-soluble inorganic salts) with refractive index of 1.559067-0.0i, 1.553280-0.0i, 1.550075-0.0i and 1.548233-0.0i, and other matters as residual (1.574-0.0026i, 1.548-00072i, 1.537-0.00094i, 1.530-0.0020i). The complex refractive indexes are calculated using a so-called mixture effective permittivity obtained from the mixture of water uptake with other three substances based on multiphase mixture theory derived from equation set of Maxwell Garnett (Sihvola, 2000).

$$m^{mix} = \sqrt{\frac{\left|\varepsilon_{eff}\right| + Re(\varepsilon_{eff})}{2}} + i\sqrt{\frac{\left|\varepsilon_{eff}\right| - Re(\varepsilon_{eff})}{2}}, \quad (3)$$

where, m^{mix} are the calculated refractive index; ε_{eff} is the effective permittivity. Mixture effective permittivities are represented by the following formula:

$$\varepsilon_{eff} = \varepsilon_e + 3\varepsilon_e \left[\frac{\sum_{n=1}^{N} f_n \frac{\varepsilon_{i,n} - \varepsilon_e}{\varepsilon_{i,n} + 2\varepsilon_e}}{1 - \sum_{n=1}^{N} f_n \frac{\varepsilon_{i,n} - \varepsilon_e}{\varepsilon_{i,n} + 2\varepsilon_e}}\right], \quad (4)$$

where, f_n is the fraction of aerosol volume, and N is the number of aerosol compositions; ε_i and ε_e are the permittivities, calculated by Eq. (3), of inclusion (here, soot, water-soluble and residual substances) and its environment (here, aerosol, water), respectively. We can obtain the refractive index from retrievals of sun-sky radiometer measurements and we can obtain the calculated one by changing columnar aerosol volume fraction (f_n) using Eqs. (3) and (4). The differences at multiple wavelengths are chosen as the iterative kernel function to solve the equation and derive the fraction of aerosol constituents:

$$\chi^2 = \sum_{\lambda=1}^{4} \frac{m_\lambda^{AERO} - m_\lambda^{mix}}{m_\lambda^{AERO}} \quad (5)$$

where, χ^2 is the refractive index error, m^{AERO} is the sun-sky radiometer retrieved refractive index, m^{mix} is the calculated (Maxwell Garnett equation) refractive index and λ is the summation index over the four retrieval wavelengths. We obtain the fraction of water uptake and others when the χ^2 is minimized. The estimated errors of aerosol composition fractions are about 30%, principally from assumptions about aerosol composition, mixing states and scattering properties (Schuster *et al.*, 2005). In this work, we mainly focus on the volume fractions of water uptake and hygroscopic aerosols.

RESULTS

Environmental Parameters and Aerosol Size Distribution

In order to investigate the growth of aerosol sizes and particle masses during haze pollution, it is important to analyse the evolution of meteorological variables including temperature, RH and horizontal velocity in the polluted and non-haze days. Fig. 1 shows these meteorological parameters on 9 and 12 January 2013. The RH on 9 January decreases slowly from 8:00 to 16:00 (local time), while RH remains above 80% before noon on 12 January and then decreases rapidly down to 60%, remaining almost constant on. The temperature is lower on 12 January while it is in general cooler along all the time period (08:00–16:00) as shown in Fig. 1(b). Fig. 1(c) presents consistent trends of the wind velocity, and indicates that rapid fluctuations associated to turbulence become intensive for higher temperatures (see Fig. 1(b)). The average wind velocity during daytime on 12 January is about 1.4 m/s, a value lower than those 2.3 m/s registered on 9 January.

The increases of both the aerosol optical depth (AOD) and particulate matter concentrations ($PM_{2.5}$) are important indicators of haze pollution, as shown in Fig. 2. The AOD increases dramatically from 0.33 to 1.63 on 12 January, with a mean value of 0.82. The aerosol mass concentration in term of $PM_{2.5}$ increases from 174 $\mu g/m^3$ at 7:00 up to 886 $\mu g/m^3$ at 20:00 on 12 January. Compared to those values obtained on haze pollution day, AOD and $PM_{2.5}$ values for the non-haze day are lower and remain stable along the day, being the mean AOD and $PM_{2.5}$ values of 0.24 and 54 $\mu g/m^3$, respectively.

Fig. 3 shows columnar aerosol volume distributions on the haze (Fig. 3(a)) and non-haze (Fig. 3(b)) days. We find that changes in aerosol distributions are weak on 9 January, with also insignificant time changes in both AOD and $PM_{2.5}$ mass concentrations during this non-haze day (see Fig 2), as stated before. However, dramatic growths of aerosols in

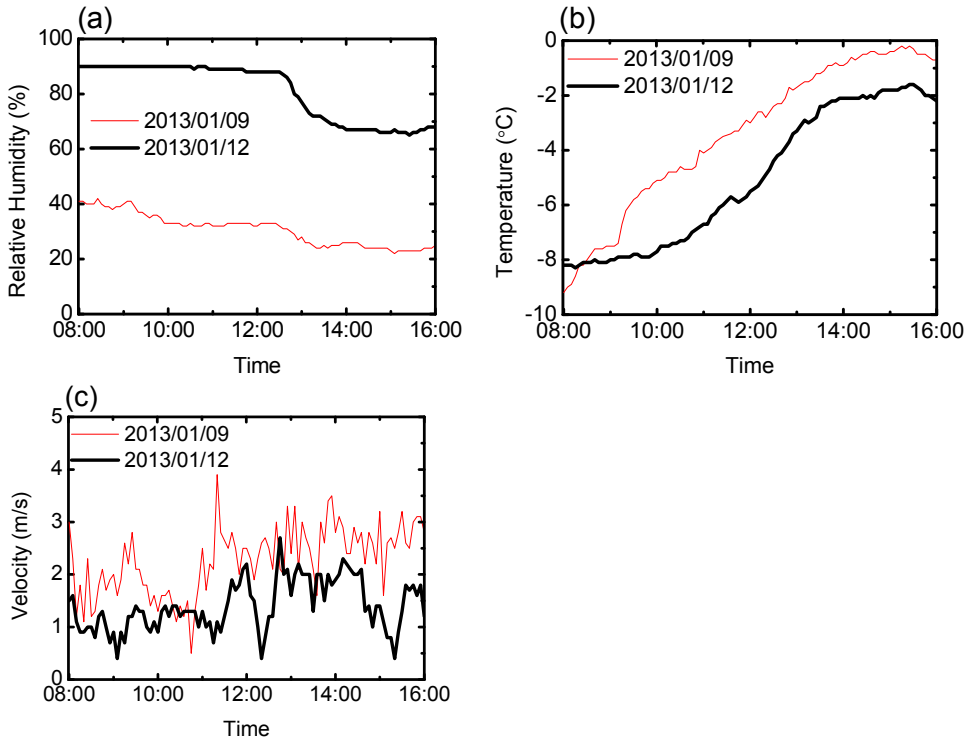

Fig. 1. Meteorological parameters registered on 9 January (non-haze day) and 12 January (haze day) 2013: (a) relative humidity, (b) temperature and (c) wind velocity.

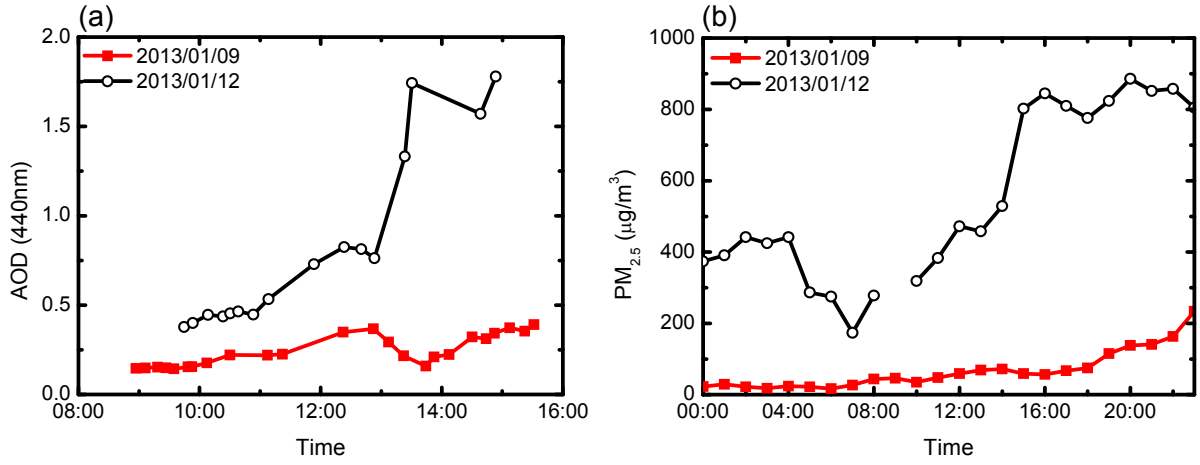

Fig. 2. (a) Aerosol optical depth (AOD) at 440 nm and (b) fine particulate matters ($PM_{2.5}$) concentrations on 9 January (non-haze day) and 12 January (haze day) 2013.

the fine and coarse mode on 12 January lead to concomitant changes in AODs and $PM_{2.5}$ concentrations. Fig. 3(b) shows that aerosol volumes in fine modes are increased rapidly from 10:24 to 13:24. On 12 January, $PM_{2.5}$ mass concentrations also increase continuously from 8:00 to 16:00. Therefore, this suggests that aerosols in fine mode may respond to the strong enhancement of $PM_{2.5}$ in the haze day, as indicated by Sun *et al.* (2013). Meanwhile, the aerosol volume in coarse mode is also increased from 12:24 to 13:24 in this case due to transported dust aerosol (discussed in section 3.6), agreeing with He *et al.* (2014). Therefore, the AOD increase in this case is linked to both the fine and coarse modal aerosols for our analysis.

Fig. 4 shows the aerosol HGRs calculated by Eq. (1) for the non-haze and haze days, respectively. During the non-haze day, HGRs are less than 0.01 $\mu m^3/\mu m^2/hr$ for Fine modes (Fig. 4(a)). Especially in VF mode, the values of HGRs are approximately equal to zero. This suggests that the accumulation aerosol in VF mode has almost no changes in the non-haze day. Although HGRs in coarse mode are around 0.01 $\mu m^3/\mu m^2/hr$, those particles cannot contribute to $PM_{2.5}$ concentrations. On 12 January (Fig. 4(b)), however, HGRs from 10:24 to 12:24 have a single maximum of 0.018 $\mu m^3/\mu m^2/hr$ peaking in the VF mode. In addition, the HGR

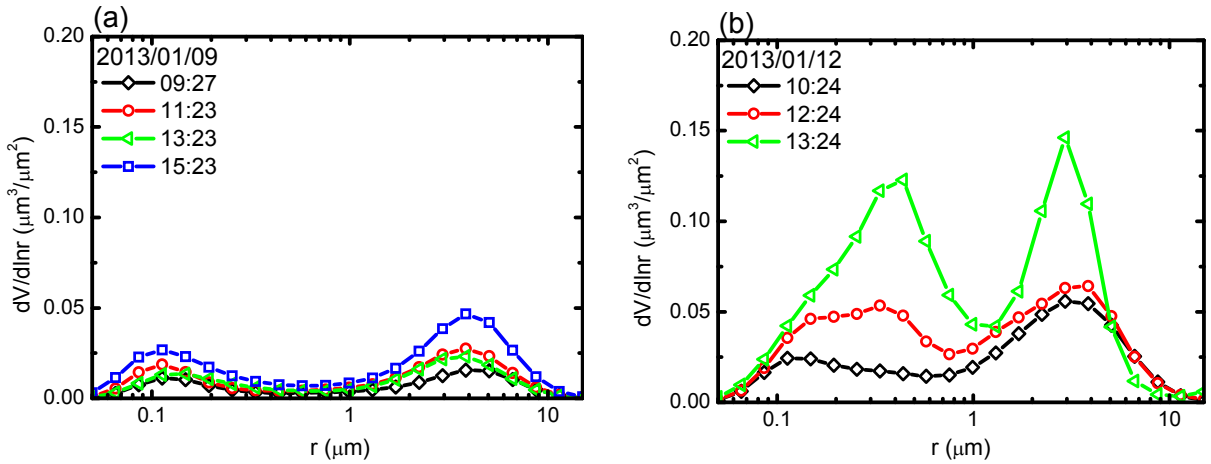

Fig. 3. Aerosol columnar volume size distribution (dV/dlnr) from AERONET ground-based measurements in Beijing on: (a) 9 January (non-haze day) and (b) 12 January (haze day).

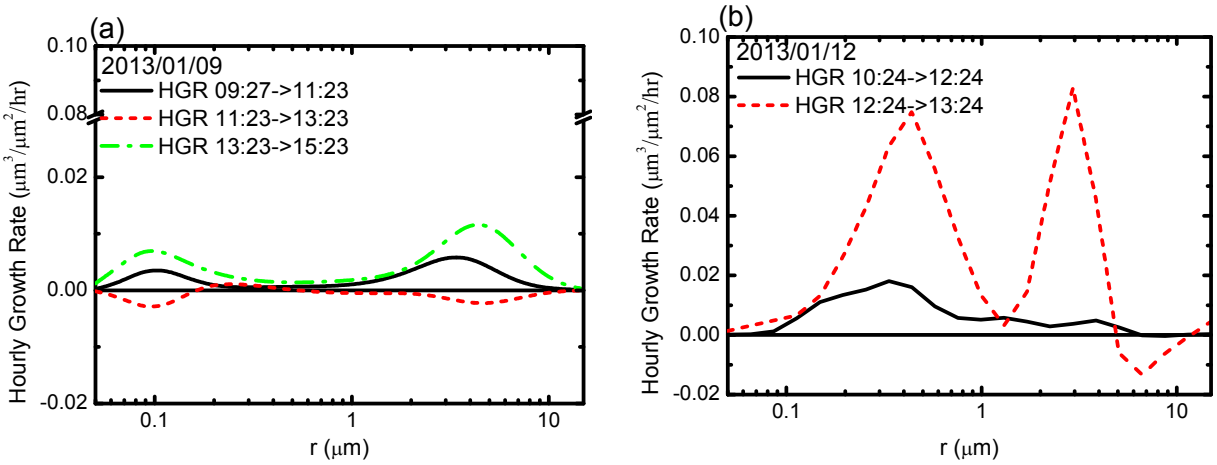

Fig. 4. Hourly growth rate (HGR) calculated by the mean hourly changes of aerosol columnar volume size distributions on: (a) 9 January (non-haze day) and (b) 12 January (haze day).

between 12:24 and 13:24 presents a bimodal distribution with the maximal values of 0.075 $\mu m^3/\mu m^2$/hr and 0.083 $\mu m^3/\mu m^2$/hr for the VF and coarse modes, respectively. Correspondingly, the AOD and $PM_{2.5}$ increase during the time interval of 13:00–13:30, being mostly remarkable for the AOD that increases from around 0.7 to 1.6 (see Fig. 2). Based on the analysis of the above, it is implied that HGR is a potential indicator to distinguish haze and non-haze days, in particular VF modal HGR.

During the earlier stage of haze (e.g., before 12:30 on 12 January), the HGR in VF mode is larger than that of other modes, but always less than 0.02 $\mu m^3/\mu m^2$/hr. And then when haze is developing (e.g., after 12:30 on 12 January), HGR in VF mode is significantly higher than 0.06 $\mu m^3/\mu m^2$/hr and the coincident remarkable increase of AOD and $PM_{2.5}$ concentrations are also observed. Comparing the HGR between earlier and developing stages of haze pollution, we find that longer time is needed in the earlier stage of haze aerosols. Indeed, the increase of HGR in VF mode can imply the formation of haze, i.e., the particles in VF mode can increase quickly in a short period (e.g., in 1 hour) or they can be advected from a neighbouring region. In addition, coarse particles also increase rapidly in this case which is explained by the deposition of floating dust from northwest as explained before.

Changes in Aerosol Size Parameters

As explained in Section 2.2.2, we apply the LNM breaking down approach (Cuesta *et al.*, 2008) to size distribution retrievals on 9 and 12 January 2013. The derived size distribution modal parameters and relative errors are listed in Table 1. Relative errors are less than 20% and the fitting parameters are in the reasonable ranges compared with those retrieved from worldwide AERONET network of ground-based radiometers (e.g., Dubovik *et al.*, 2002).

In Table 1, we can see that fine modal radii (including QCF and VF modes) are between 0.1 and 0.2 μm, and coarse modal radii are larger than 3.0 μm during the non-haze day on 9 January 2013. The mean radius is 0.14 and 3.6 μm, respectively, for the fine and coarse modes on non-haze day. However, the fine modal radii on the haze day changes mostly from 0.2 to 0.36 μm, with the mean value

Table 1. Modal parameters of the aerosol volume size distributions calculated for both fine (f) and coarse (c) modes by log-normal breaking down approach on 9 January (non-haze day) and 12 January (haze day) 2013.

Date	Time	AODs (@440 nm)	r_f (μm)	r_c (μm)	σ_f	σ_c	Residual (%)
2013/1/9	09:27	0.15	0.14	3.78	1.67	1.85	18.48
	11:23	0.23	0.12	3.50	1.57	1.80	17.15
	13:23	0.22	0.16	3.37	1.92	1.78	12.43
	15:23	0.37	0.13	3.76	1.95	1.75	14.31
	Mean	0.24	0.14	3.60	1.78	1.80	--
2013/1/12	10:24	0.45	0.20	3.00	2.40	1.89	9.23
	12:24	0.82	0.12/0.32	2.96	1.35/2.00	1.85	6.26
	13:24	1.54	0.36	2.95	2.13	1.43	8.03
	Mean	0.94	0.29	2.97	2.18	1.73	--

Note: r_f is the fine modal radius for the fine mode of the size distribution. However, a tri-modal distribution is presented at 12:24 on 12 January 2013 with modal radii of 0.12 and 0.32 in quasi-conservative (QC) and variable fine (VF) modes, respectively and thus two values of r_f and σ_f are shown.

of 0.29 μm. In addition, a tri-modal size distribution is observed at 12:24. It indicates that particle sizes during haze pollution can increase from QCF mode to VF mode due to enhancements on RH and water-soluble matters compared with those during non-haze day (on 9 January), in agreement with Li *et al.* (2014). In contrast, the RH decreases after 12:30 on 12 January may result from the increase of temperature and particles size related to the water uptake by the fine particles (from QCF to VF mode). The coarse modal radii slightly changes around 3.0 μm on 12 January. The standard deviations of aerosol size distributions on 9 January are ranging from 1.57 to 1.95 for fine mode and from 1.75 to 1.85 for coarse modes, respectively, being mean values of 1.78 and 1.80, respectively. As compared to these non-haze values, the mean fine modal standard deviation is higher (2.18) on the haze day, and σ_c shows no obvious differences except for that registered at 13:24.

Fig. 5 shows the relationship between the AOD at 440 nm and fine/coarse modal radii on the haze and non-haze days. A good correlation (R^2 = 0.92) between AOD and fine modal radii is found with slope of 0.17 and intercept of 0.11, while the negative correlation between AOD and coarse modal radii is also presented, with slope of –0.53. Meanwhile, the mean r_f on 12 January (haze day) respect to 9 January (non-haze day) increased from 0.14 to 0.29 while the mean r_c decreased from 3.60 to 2.97. It suggests that the fine and coarse aerosol fractions, respectively, present a larger and smaller modal size in average on haze day respect to those values obtained on non-haze day (lower AODs). The aerosol fine (QCF and VF) modal radius (r_f) obviously increase with AOD during haze day, but coarse modal radius (r_c) is held nearly constant. Dubovik *et al.* (2002) found the same results for fine modes, being the maximum slope of about 0.13 as calculated with the data from Crete-Paris, France on 1999. Presumably, the larger size of fine modal aerosol would be a combined effect of higher aerosol water uptake due to the existence of more water-soluble aerosol matters and transformations such as coagulation, agglomeration of particles and formation of secondary aerosols prevailing during the haze pollution events, as well.

Changes in Aerosol Compositions

Fig. 6 shows the daily average volumes of aerosol compositions, calculated from the composition volume fraction f_n obtained from Eq. (4) and the total columnar-integrated volume on the non-haze and haze days, respectively. The volume of the water-soluble matters increases from 0.017 (non-haze day) to 0.152 $\mu m^3/\mu m^2$ (haze day), about 9 times

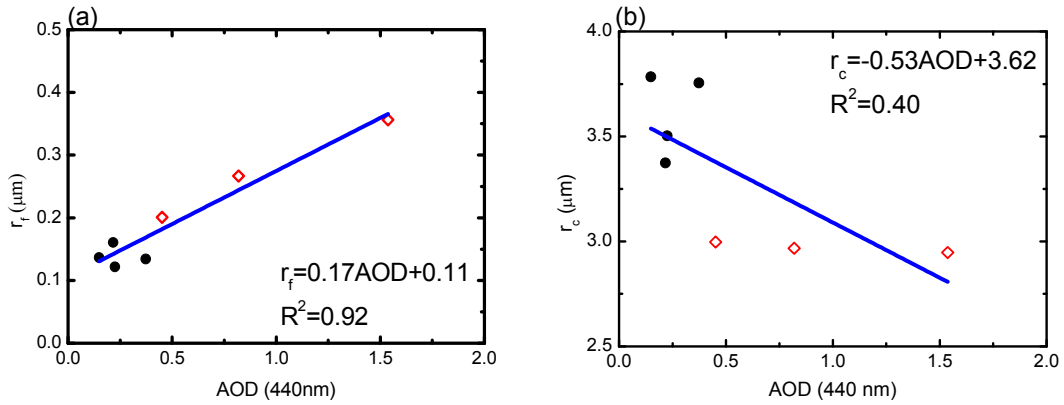

Fig. 5. Correlation between the aerosol optical depth (AOD) at 440 nm and (a) fine and (b) coarse modal radius during the haze (hollow points) and non-haze (solid points) days. The fine and coarse modal radius is derived from the aerosol columnar size distribution retrieved from the ARONET ground-based measurements.

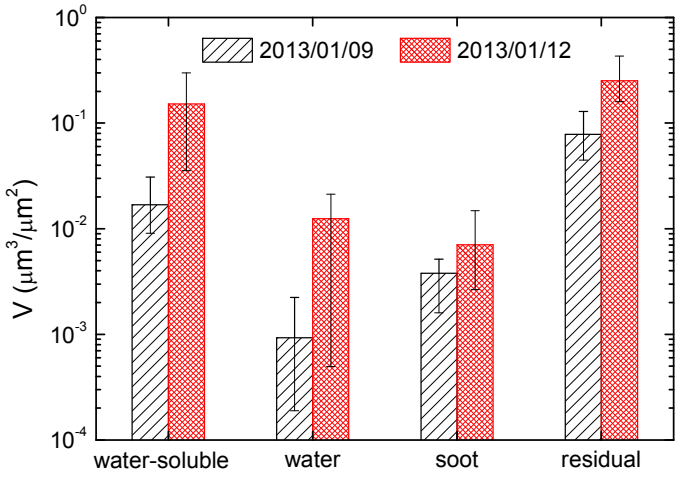

Fig. 6. The daily average volume of aerosol compositions retrieved for the non-haze (9 January) and haze (12 January) days. The x-axis of plot represents the aerosol compositions including water-soluble substance, water uptake, soot, and other matters (residual), respectively. The y-axis of plot represents the aerosol composition volume calculated by product of the volume fraction of compositions and the integral of total volume aerosol size distribution.

higher. Meanwhile, the volume of water absorbed by particles (water uptake) also increases from 0.001 (non-haze day) to 0.013 $\mu m^3/\mu m^2$ (haze day), about 13 times larger. These variations in water-soluble matters and water uptake between non-haze and haze days are mainly caused by different aerosol sources and RH. The increase of soot volumes are not large (from 0.004 to 0.007 $\mu m^3/\mu m^2$) respect to other compositions, but significant. Since BC does not involve in chemistry reactions, as a tracer, it shows that the fine aerosol columnar volume changes resulting from meteorological factors during the haze day (12 January) is about 1.75 times larger, respect to that on non-haze day (9 January). In addition, as compared to the non-haze day, the residual volumes on haze day are about 3 times larger due to the higher total aerosol volumes. Residual component in this study is assumed to be a mixture of matters different from water uptake, soot and water-soluble inorganic substances.

Fig. 7 shows the changes in water uptake and water-soluble matters on 9 and 12 January. Water uptake reduces as temperature increases on the non-haze day, as well as RH decreases too (Fig. 7(a)). The volume peak value of hygroscopic aerosols (i.e., water-soluble matters) is 0.031 $\mu m^3/\mu m^2$ while all others are considerable low on 9 January (also listed in Table 2). These results can be explained by the weaker secondary reactions while the growth of water-soluble substances is limited by the decreases in water, or aerosols transported from relatively clear areas. However, in the cases of RH values higher than 80%, as occurring on 12 January, the volumes of water uptake increase significantly up to 0.021 $\mu m^3/\mu m^2$ from 10:24 to 12:24 (Fig. 7(b)). The water-soluble aerosol matters volume increases dramatically from 0.036 to 0.298 $\mu m^3/\mu m^2$ between 10:24 and 13:24, but the volume of water uptake changes only a little at noon (see in Table 2 from 12:24 to 13:24) due to the decrease in RH. These results indicate that secondary reactions are important in the process of water-soluble substance formation, such as gas-phase formation and in-cloud formation. Meanwhile, aerosol hygroscopic growth can provide liquid surfaces for secondary chemical reactions by the increase in water content. The water-soluble substances are formed rapidly when the liquid surfaces exist in evolution stage of haze. This phenomenon was also observed and simulated by He *et al.* (2014). A large number of aerosol particles containing water-soluble substances and mineral dust deposited during haze pollution, leads to the dramatic AOD increasing on 12 January. However, we find that the increases in $PM_{2.5}$ concentrations lag behind the trend of AOD in this case. This is likely linked to the fact that mineral dust deposits near the ground in the afternoon which increases the AOD, and water-soluble substances from secondary reactions are not stable and decomposed because of the particle samples heating by the monitoring instrument (Ayers *et al.*, 1999) which can decrease $PM_{2.5}$ during haze condition.

The mean net effect of water uptake on the AOD, as difference calculated using a Mie code with and without water uptake (results also in changes of refractive index and size distribution) is in average 0.023 and 0.047 for the non-haze (9 January) and haze (12 January) days, respectively (see in Table 2). In particular, the net effect is 0.057 at 13:24 on 12 January, for a water uptake volume of 0.021 $\mu m^3/\mu m^2$. Calculations show a negative effect of –0.003 at 12:24 for the haze day, since the decrease in particle size due to water loss here is only calculated by single particle hygroscopic growth while the changes of size distribution shape cannot be captured. Except for the negative value, the net effect of water uptake in AOD is 0.023 on the non-haze day and relatively as higher as 0.047 on the haze day due to increase in water uptake.

Correlation between Water Uptake and Water-Soluble Matters

In Fig. 8, we present the aerosol composition retrieved for the whole month of January 2013 in order to obtain the

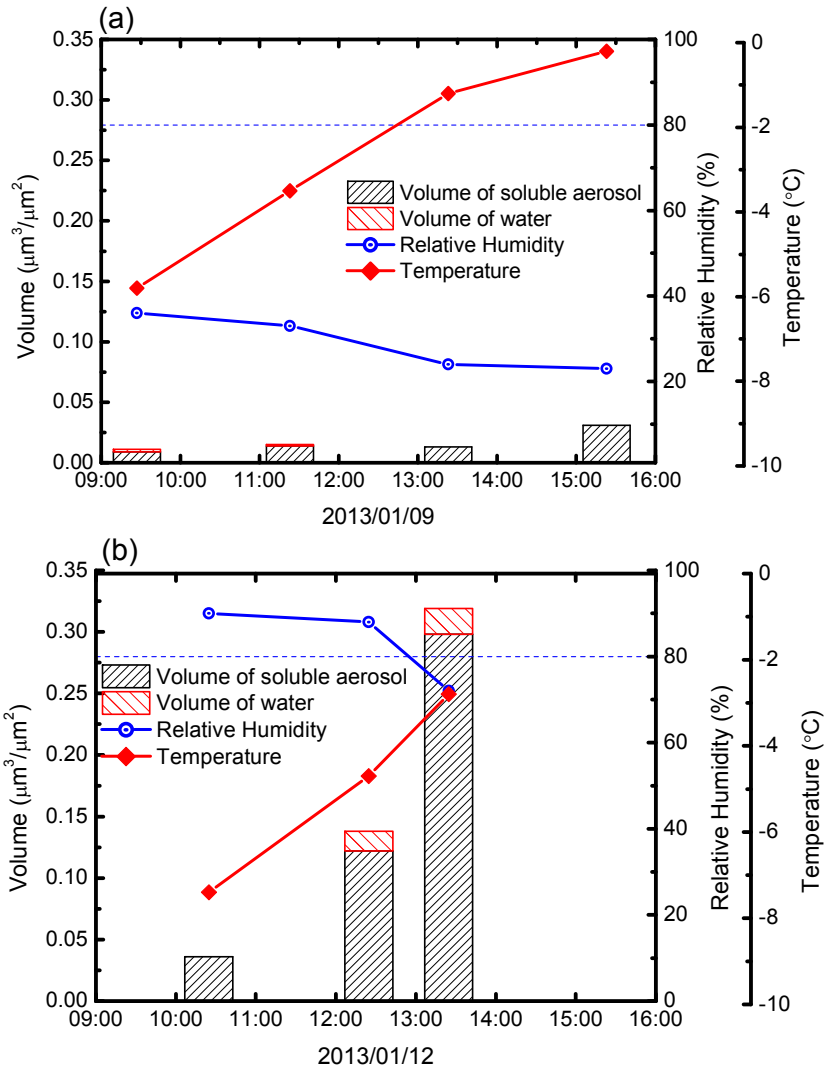

Fig. 7. Daily variations of water uptake and hygroscopic compositions, and changes of relative humidity and temperature corresponding to observation of AERONET ground-based radiometer on: (a) 9 January (non-haze day) and (b) 12 January(haze day).

Table 2. Volume of aerosol water-soluble substance and water uptake, together with meteorological parameters and the net effect of water uptake (WU) on AOD during the non-haze (9 January) and haze (12 January) day.

Volume	2013/01/09					2013/01/12			
($\mu m^3/\mu m^2$)	9:27	11:23	13:23	15:23	Mean	10:24	12:24	13:24	Mean
Water-soluble	0.009	0.014	0.013	0.031	0.017	0.036	0.122	0.298	0.152
Water uptake	0.002	0.001	1.886E-04	4.301E-04	0.001	4.951E-04	0.016	0.021	0.013
Net effect of WU on AOD	0.020	0.011	0.023	0.038	0.023	0.038	–0.003	0.057	0.047
RH (%)	36	33	24	23	--	90	88	72	--
T (°C)	–5.8	–3.5	–1.2	-0.2	--	–7.4	–4.7	–2.8	--

prevailing correlation between water uptake and water-soluble matter in all conditions (including non-haze and haze days). A fairly good correlation between water-soluble aerosol matter and water uptake can be found, with the correlation coefficient (r) of 0.66. It is indicated that the water uptake can lead to increase in the water-soluble substances. However, water in aerosols could be evaporated when RH is low as that on 9 January (non-haze day), and expended when RH decreases rapidly due to heavy pollution as that on 12 January (haze day), in particular in winter over North China. Generally, although aerosols are emitted from different sources and transported from different areas in January 2013, the fitting line shows that water-soluble volume increases with increasing water volume, and water-soluble volumes are larger than 0.05 $\mu m^3/\mu m^2$ for water volumes beyond 0.01 $\mu m^3/\mu m^2$.

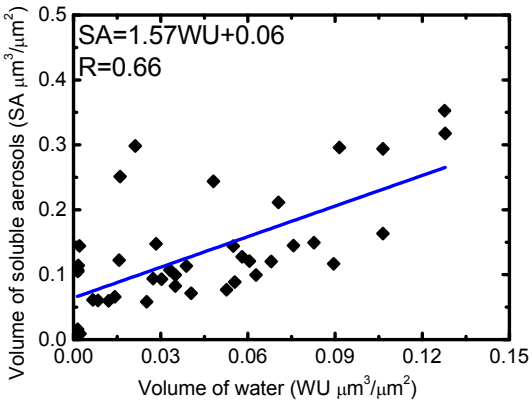

Fig. 8. Correlation between volumes of water (WU: water uptake) and hygroscopic compositions (SA: soluble aerosols) in January 2013. Solid line is the best fitting line for volumes of water uptake higher than 0.01 $\mu m^3/\mu m^2$.

Comparison of Retrieved Soot Mass with Surface Measurements

We compared the soot mass concentrations retrieved from AERONET sun-sky radiometer observations with surface measurements by aethalometer at Beijing in January 2013 (Fig. 9). If a 1.8 g/cm^3 density of soot (midrange value of 1.7–1.9 g/cm^3 in Bond and Bergstrom, 2005) is assumed, daily-averaged soot mass concentrations from two data set have a fairly good correlation coefficient (r) of 0.77. This indicates that the columnar retrievals of soot mass, to a certain degree, could reflect the changes of soot at surface. Assuming a boundary layer of 1 km height (Lv *et al.*, 2013), we can convert the retrieved daily average columnar soot mass to the surface quantity which in this case has also a good correlation (r = 0.63) with aethalometer measurements. The converted soot mass from the retrieval presents slightly higher values than those registered by surface measurements, with a mean error of 2.59 $\mu g/m^3$. Moreover, the time variation of the retrieved soot mass concentration also agrees well with surface observations.

Influence of Sources on Particle Size Distribution and Compositions

The aerosol size distributions and compositions greatly depend on aerosol sources. Fig. 10 shows 48-h backward trajectories of air masses reaching Beijing on the heights of 10, 500, 1000 and 2000 meters above ground level on 9 January (ending at 9:00, 11:00, 13:00 and 15:00 local time) and 12 January (ending at 10:00, 11:00, 12:00 and 13:00). It can be seen in Fig. 10(a) that aerosols in air masses come from northwest direction, mainly including Hebei and Inner Mongolia provinces of China, Mongolia and Russia, and aerosols are transported from altitudes higher than 2 km 48 hours before arrival on 9 January (Fig. 10(c)). The higher aerosol transport speed and height together lead to a lower aerosol loading until 10 January. However, more aerosols reach Beijing on the haze day (12 January) due to lower transport height (less than 2 km) since 11 January (Fig. 10(d)), with the direction of air flow from western Hebei, northern Shanxi and Inner Mongolia provinces and Mongolia (Fig. 10(b)). In particular on 12 January, aerosols are mainly emitted from local sources because of the arrival of air masses at lower heights leading to reduced long-range transport of pollutants (Fig. 10(d)). The coarse modal particles can be transported from northwest direction above 2 km height, declining and depositing near Beijing due to wind speed decrease (see Fig. 1(c)).

The aerosol size distributions from different sources can have distinct properties. Lee and Kim (2010) presented aerosol size distributions from 20 AERONET city sites including Beijing in East Asia and classified them into six

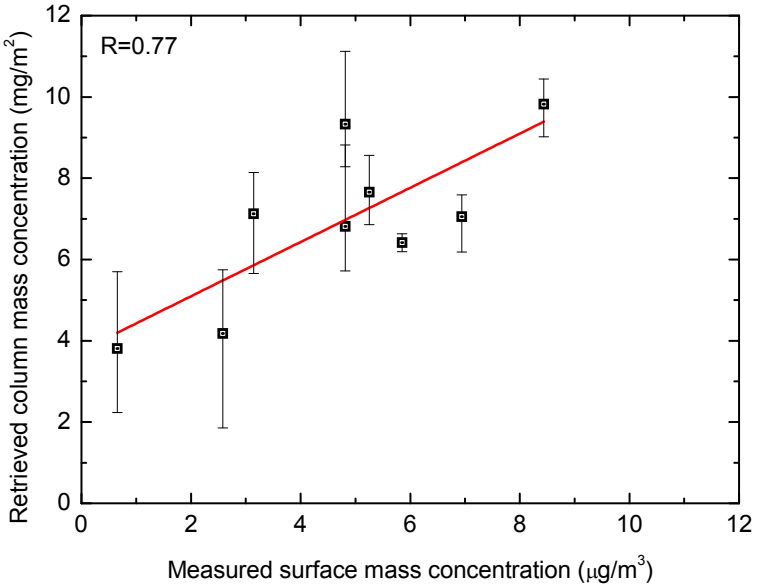

Fig. 9. The daily average columnar soot mass concentration obtained from remote sensing retrievals and surface measurements by aethalometer during January 2013 in Beijing. Error bars show the maximum and minimum values of soot mass concentration obtained in each day.

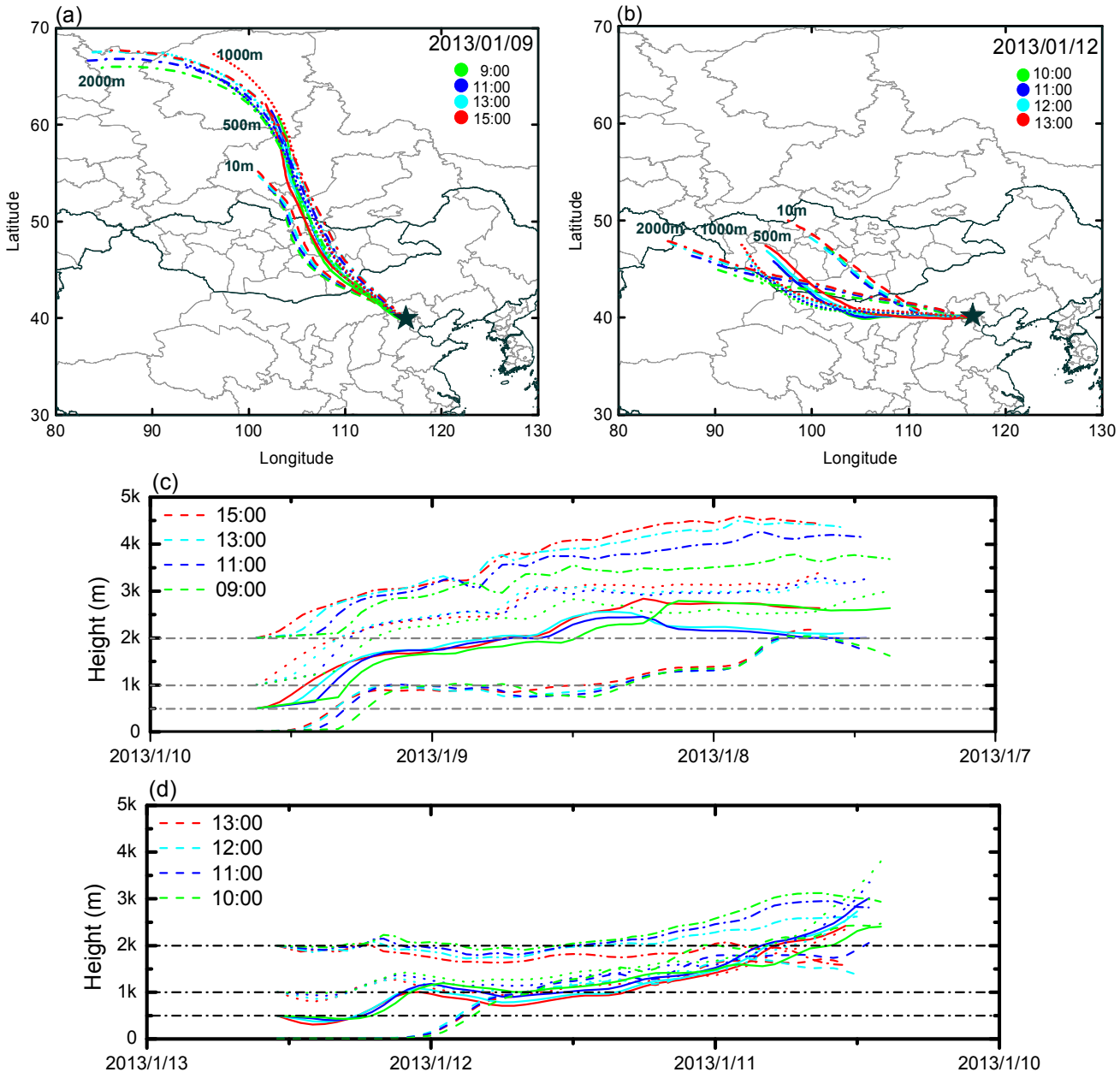

Fig. 10. 48-h backward trajectories of air masses reaching Beijing at selected heights: 10, 500, 1000 and 2000 meters above ground level ending at 9:00, 11:00, 13:00 and 15:00 on 9 January (a and c) and 10:00, 11:00, 12:00 and 13:00 on 12 January (b and d).

categories with different optical and microphysical parameters using cluster analysis technique. They found that the maximum of fine modal radii in six categories is 0.257 μm and identified as urban/industrial pollution, since it is a higher value than that corresponding to dusty aerosols. In our study, the fine modal radii on the non-haze day are all less than 0.16 μm, which is the minimal value of the fine radii of dusty aerosols in Lee and Kim's classification, and there are nearly no significant variations in fine and coarse modal radii on 9 January. However, the fine modal radii on 12 January (haze day) are higher than 0.257 μm, except for that obtained at 10:24. These results suggest that the impacts of RH on particulate size occur mainly in haze days instead of non-haze conditions, as previously stated.

Different sources can also affect aerosol compositions. The crustal matters are dominated in aerosols transported from Mongolia (Natsagdorj *et al.*, 2003), because more than 70% of the pastureland area of Mongolia is under desertification (Jigjidsuren and Oyuntsetseg, 1998). However, mass concentrations of hygroscopic aerosols including sulfate, nitrate and ammonium can account for more than 25% of $PM_{2.5}$ mass concentrations in Beijing (Duan *et al.*, 2006). It is thus suggested that there are more hygroscopic aerosols emitted into atmosphere from local sources in Beijing, rather than transported from Mongolia. Assuming such kind of local sources and their diffusion are stable

(this is reasonable considering wind speeds less than 1.5 m/s on 12 January), the significant AOD and $PM_{2.5}$ increases on haze day are most likely explained by RH effects instead of aerosol source emission changes.

DISCUSSIONS AND CONCLUSIONS

Beijing is one of the largest megacities in China and is polluted due to high emissions of pollutants and precursors associated to the fast development of economy. The aerosol properties during the seriously polluted day on 12 January 2013, as compared to the non-haze day on 9 January, are investigated focusing on the evolution of haze pollution. In this work, aerosol columnar size distribution parameters and aerosol compositions are calculated from aerosol optical depths, aerosol volume size distributions, and complex refractive indexes obtained from ground-based remote sensing measurements.

The impacts of haze pollution on aerosol properties are quantified to exhibit aerosol size distribution and water-soluble substance variations. The changes in aerosol size distributions during haze day are obtained from the hourly growth rate (HGR). The HGR in the fine mode increase significantly during the haze day while it almost equals to zero in the non-haze day, which could be used as a reference to monitor the development of haze pollution. Meanwhile, variations in the fine-mode peak radius, another important size distribution parameter, present significant differences between the haze and non-haze day, e.g., 0.29 versus 0.14 μm. Aerosol in fine mode with larger size on haze day is explained by the increase of water uptake, while it has also a smaller size in the coarse mode. For aerosol compositions, the volume growth of aerosol water-soluble substances can be 9 times higher and water uptake can be 13 times greater on haze day than non-haze day. In the study period, the air quality deterioration near the surface in haze day is mainly caused by increasing of fine modal aerosols because of high RH leading to particle hygroscopic growth. Moreover, the impact of meteorological factor changes on aerosol increases during air pollution, estimated by the increases of black carbon considering its neutrality in chemical reactions, is smaller than that of hygroscopic growth and secondary reactions. In addition, further studies can be focused on combining multiple methods of remote sensing like LIDAR and improving the accuracy of aerosol composition retrievals.

ACKNOWLEDGEMENTS

This work was supported by the National Basic Research Program of China (973 program) under Grant No. 2010CB950800 (2010CB950801), the Chinese Academy of Sciences Key Deployment project (No. KZZD-EW-TZ-18), and National Natural Science Fund of China (No. 41222007).

REFERENCES

Arola, A., Schuster, G., Myhre, G., Kazadzis, S., Dey, S., and Tripathi, S.N. (2011). Inferring Absorbing Organic Carbon Content from AERONET data. *Atmos. Chem. Phys.* 11: 215–225.

Ayers, G.P., Keywood, M.D. and Gras, J.L. (1999). TEOM vs. Manual Gravimetric Methods for Determination of $PM_{2.5}$ Aerosol Mass Concentrations. *Atmos. Environ.* 33: 3717–3721.

Betha, R., Spracklen, D.V. and Balasubramanian, R. (2013). Observations of New Aerosol Particle Formation in a Tropical Urban Atmosphere. *Atmos. Environ.* 71: 340–351.

Bond, T.C. and Bergstrom, R.W. (2005). Light Absorption by Carbonaceous Particles: An Investigative Review. *Aerosol Sci. Technol.* 39: 1–41.

Brook, R.D., Rajagopalan, S., Pope, C.A., Brook, J.R., Bhatnagar, A., Diez-Roux, A.V., Holguin, F., Hong, Y.L., Luepker, R.V., Mittleman, M.A., Peters, A., Siscovick, D., Smith, S.C., Whitsel, L. and Kaufman, J.D. (2010). Particulate Matter Air Pollution and Cardiovascular Disease an Update to the Scientific Statement from the American Heart Association. *Circulation* 121: 2331–2378.

Chen, L.W.A., Chow, J.C., Doddridge, B.G., Dickerson, R.R., Ryan, W.F. and Mueller, P.K. (2003). Analysis of a Summertime $PM_{2.5}$ and Haze Episode in the Mid-Atlantic Region. *J. Air Waste Manage. Assoc.* 53: 946–956.

Cheng, Y.F., Eichler, H., Wiedensohler, A., Heintzenberg, J., Zhang, Y.H., Hu, M., Herrmann, H., Zeng, L.M., Liu, S., Gnauk, T., Bruggemann, E. and He, L.Y. (2006). Mixing State of Elemental Carbon and Non-light-absorbing Aerosol Components Derived from in Situ Particle Optical Properties at Xinken in Pearl River Delta of China. *J. Geophys. Res.* 111, doi: 10.1029/2005JD006929.

Cheng, Y.F., Wiedensohler, A., Eichler, H., Heintzenberg, J., Tesche, M., Ansmann, A., Wendisch, M., Su, H., Althausen, D., Herrmann, H., Gnauk, T., Bruggemann, E., Hu, M. and Zhang, Y.H. (2008a). Relative Humidity Dependence of Aerosol Optical Properties and Direct Radiative Forcing in the Surface Boundary Layer at Xinken in Pearl River Delta of China: An Observation Based Numerical Study. *Atmos. Environ.* 42: 6373–6397.

Cheng, Y.F., Wiedensohler, A., Eichler, H., Su, H., Gnauk, T., Brueggemann, E., Herrmann, H., Heintzenberg, J., Slanina, J., Tuch, T., Hu, M. and Zhang, Y.H. (2008b). Aerosol Optical Properties and Related Chemical Apportionment at Xinken in Pearl River Delta of China. *Atmos. Environ.* 42: 6351–6372.

Chu, D.A., Tsai, T.C., Chen, J.P., Chang, S.C., Jeng, Y.J., Chiang, W.L. and Lin, N.H. (2013). Interpreting Aerosol LIDAR Profiles to Better Estimate Surface $PM_{2.5}$ for Columnar AOD Measurements. *Atmos. Environ.* 79: 172–187.

Chýlek, P. and Coakley, J.A. (1974). Aerosol and Climate. *Science* 183: 7–9.

Cuesta, J., Flamant, P.H. and Flamant, C. (2008). Synergetic Technique Combining Elastic Backscatter Lidar Data and Sun Photometer AERONET Inversion for Retrieval by Layer of Aerosol Optical and Microphysical Properties. *Appl. Opt.* 47: 4598–4611.

Dockery, D.W. and Pope, C.A. (1994). Acute Respiratory Effects of Particulate Air-Pollution. *Auun. Rev. Publ. Health* 15: 107–132.

Du, H., Kong, L., Cheng, T., Chen, J., Du, J., Li, L., Xia, X., Leng, C. and Huang, G. (2011). Insights into Summertime Haze Pollution Events over Shanghai Based on Online Water-soluble Ionic Composition of Aerosols. *Atmos. Environ*. 45: 5131–5137.

Duan, F.K., He, K.B., Ma, Y.L., Yang, F.M., Yu, X.C., Cadle, S.H., Chan, T. and Mulawa, P.A. (2006). Concentration and Chemical Characteristics of $PM_{2.5}$ in Beijing, China: 2001-2002. *Sci. Total Environ.* 355: 264–275.

Dubovik, O., Smirnov, A., Holben, B.N., King, M.D., Kaufman, Y.J., Eck, T.F. and Slutsker, I. (2000). Accuracy Assessments of Aerosol Optical Properties Retrieved from Aerosol Robotic Network (AERONET) Sun and Sky Radiance Measurements. *J. Geophys. Res.* 105: 9791–9806.

Dubovik, O., Holben, B., Eck, T.F., Smirnov, A., Kaufman, Y.J., King, M.D., Tanre, D. and Slutsker, I. (2002). Variability of Absorption and Optical Properties of Key Aerosol Types Observed in Worldwide Locations. *J. Atmos. Sci.* 59: 590–608.

He, H., Wang, Y., Ma, Q., Ma, J., Chu, B., Ji, D., Tang, G., Liu, C., Zhang, H. and Hao, J. (2014). Mineral Dust and No_x Promote the Conversion of SO_2 to Sulfate in Heavy Pollution Days. *Sci. Rep.* 4: 4172, doi: 10.1038/srep0472.

IPCC (2013). *Climate Change 2013: The Physical Science Basis. Contribution of Working Group I to the Fifth Assessment Report of the Intergovernmental Panel on Climate Change*, Stocker, T.F., Qin, D., Plattner, G.K., Tignor, M., Allen, S.K., Boschung, J., Nauels, A., Xia, Y., Bex, V. and Midgley, P.M. (Eds.), Cambridge University Press, Cambridge, United Kingdom and New York, NY, USA, 1535 pp, doi: 10.1017/CBO9781107415324.

Jigjidsuren, S. and Oyuntsetseg, S. (1998). Pastureland Utilization Problems and Ecosystem. *Ecol. Sustainable Dev.* 2: 206–212.

Kang, E., Han, J., Lee, M., Lee, G. and Kim, J.C. (2013a). Chemical Characteristics of Size-resolved Aerosols from Asian Dust and Haze Episode in Seoul Metropolitan City. *Atmos. Res.* 127: 34–46.

Kang, H., Zhu, B., Su, J., Wang, H., Zhang, Q. and Wang, F. (2013b). Analysis of a Long-lasting Haze Episode in Nanjing, China. *Atmos. Res.* 120–121: 78–87.

Kunzli, N., Jerrett, M., Mack, W.J., Beckerman, B., LaBree, L., Gilliland, F., Thomas, D., Peters, J. and Hodis, H.N. (2005). Ambient Air Pollution and Atherosclerosis in Los Angeles. *Environ. Health Perspect.* 113: 201–206.

Lee, K.H. and Kim, Y.J. (2010). Satellite Remote Sensing of Asian Aerosols: A Case Study of Clean, Polluted, and Asian Dust Storm Days. *Atmos. Meas. Tech.* 3: 1771–1784.

Li, Z., Gu, X., Wang, L., Li, D., Xie, Y., Li, K., Dubovik, O., Schuster, G., Goloub, P., Zhang, Y., Li, L., Ma, Y. and Xu, H. (2013a). Aerosol Physical and Chemical Properties Retrieved from Ground-based Remote Sensing Measurements during Heavy Haze Days in Beijing Winter. *Atmos. Chem. Phys.* 13: 10171–10183.

Li, Z., Xu, H., Zhang, Y., Zhang, Y.H., Chen, C., Li, D.H., Hou, W.Z., Lv, Y. and Gu, X. (2013b). Joint Use of Active and Passive Remote Sensing for Monitoring of Severe Haze Pollution in Beijing. *J. Remote Sens.* 17: 919–928.

Li, Z.Q., Eck, T., Zhang, Y., Zhang, Y.H., Li, D.H., Li, L., Xu, H., Hou, W.Z., Lv, Y., Goloub, P. and Gu, X.F. (2014). Observation of Residual Submicron Fine Aerosol Particles Related to Cloud and Fog Processing during a Major Pollution Event in Beijing. *Atmos. Environ.* 86: 187–192.

Liu, X.G., Cheng, Y.F., Zhang, Y.H., Jung, J.S., Sugimoto, N., Chang, S.Y., Kim, Y.J., Fan, S.J. and Zeng, L.M. (2008). Influences of Relative Humidity and Particle Chemical Composition on Aerosol Scattering Properties during the 2006 PRD Campaign. *Atmos. Environ.* 42: 1525–1536.

Liu, X.G., Li, J., Qu, Y., Han, T., Hou, L., Gu, J., Chen, C., Yang, Y., Liu, X., Yang, T., Zhang, Y., Tian, H. and Hu, M. (2013). Formation and Evolution Mechanism of Regional Haze: A Case Study in the Megacity Beijing, China. *Atmos. Chem. Phys.* 13: 4501–4514.

Lv, Y., Li, Z.Q., Xu, H., Li, K.T., Zhang, W.C. and Hou, W.Z. (2013). Joint Use of Ground-based Lidar and Sun-sky Radiometer for Observation of Aerosol Vertical Distribution. *J. Remote Sens.* 17: 1008–1020, doi: 10.11834/jrs.20133092.

Morin, S., Sander, R. and Savarino, J. (2011). Simulation of the Diurnal Variations of the Oxygen Isotope Anomaly (Delta O-17) of Reactive Atmospheric Species. *Atmos. Chem. Phys.* 11: 3653–3671.

Nakajima, T., Tanaka, M. and Yamauchi, T. (1983). Retrieval of the Optical Properties of Aerosols from Aureole and Extinction Data. *Appl. Opt.* 22: 2951–2959.

Nakajima, T., Tonna, G., Rao, R., Boi, P., Kaufman, Y. and Holben, B. (1996). Use of Sky Brightness Measurements from Ground for Remote Sensing of Particulate Dispersion. *Appl. Opt.* 35: 2672–2686.

Natsagdorj, L., Jugder, D. and Chung, Y.S. (2003). Analysis of Dust Storms Observed in Mongolia during 1937–1999. *Atmos. Environ.* 37: 1401–1411.

Phoothiwut, S. and Junyapoon, S. (2013). Size Distribution of Atmospheric Particulates and Particulate-bound Polycyclic Aromatic Hydrocarbons and Characteristics of PAHs during Haze Period in Lampang Province, Northern Thailand. *Air Qual. Atmos. Health* 6: 397–405.

Pope, C.A., Burnett, R.T., Thun, M.J., Calle, E.E., Krewski, D., Ito, K. and Thurston, G.D. (2002). Lung Cancer, Cardiopulmonary Mortality, and Long-term Exposure to Fine Particulate Air Pollution, *J. Am. Med. Assoc.* 287: 1132–1141.

Schuster, G.L., Dubovik, O., Holben, B.N. and Clothiaux, E.E. (2005). Inferring Black Carbon Content and Specific Absorption from Aerosol Robotic Network (AERONET) Aerosol Retrievals. *J. Geophys. Res.* 110, doi: 10.1029/2004JD004548.

Schuster, G.L., Lin, B. and Dubovik, O. (2009). Remote Sensing of Aerosol Water Uptake. *Geophys. Res. Lett.* 36, doi: 10.1029/2008GL036576.

Seifeld, J.H. and Pandis, S.N. (2006). *Atmospheric Chemistry and Physics: from Air Pollution to Climate Change*, John Wiley & Sons, Inc., Hoboken, New Jersey.

Sihvola, A. (2000). Mixing Rules with Complex Dielectric

Coefficients. *Subsurface Sens. Technol. Appl.* 1: 393–415.
Sipe, J.E. and Boyd, R.W. (1992). Nonlinear Susceptibility of Composite Optical Materials in the Maxwell Garnett Model. *Phys. Rev. A* 46: 1614–1629.
Stelson, A.W. and Seinfeld, J.H. (1982). Relative-humidity and Temperature-dependence of the Ammonium-nitrate Dissociation-constant. *Atmos. Environ.* 16: 983–992.
Sun, Y.L., Zhuang, G.S., Tang, A.H., Wang, Y. and An, Z.S. (2006). Chemical Characteristics of $PM_{2.5}$ and PM_{10} in Haze-fog Episodes in Beijing. *Environ. Sci. Technol.* 40: 3148–3155.
Sun, Z., Mu, Y., Liu, Y. and Shao, L. (2013). A Comparison Study On airborne Particles during Haze Days and Non-Haze Days in Beijing. *Sci. Total Environ.* 456–457: 1–8.
Tan, H., Yin, Y., Gu, X., Li, F., Chan, P.W., Xu, H., Deng, X. and Wan, Q. (2013). An Observational Study of the Hygroscopic Properties of Aerosols over the Pearl River Delta Region. *Atmos. Environ.* 77: 817–826.
Wang, L., Li, Z.Q., Tian, Q.J., Ma, Y., Zhang, F.X., Zhang, Y., Li, D.H., Li, K.T. and Li, L. (2013). Estimate of Aerosol Absorbing Components of Black Carbon, Brown Carbon, and Dust from Ground-based Remote Sensing Data of Sun-sky Radiometers. *J. Geophys. Res.* 118: 6534–6543.
Wang, X. and Shi, G. (2000). A Numerical Study on Temporal and Spatial Variations of Anthropogenic Sulfate Column Burden over Eastern Asia. *Clim. Environ. Res.* 5: 58–66.
Wang, Y., Zhuang, G.S., Sun, Y.L. and An, Z.S. (2006). The Variation of Characteristics and Formation Mechanisms of Aerosols in Dust, Haze, and Clear Days in Beijing. *Atmos. Environ.* 40: 6579–6591.
Wu, D., Tie, X.X., Li, C.C., Ying, Z.M., Lau, A.K.H., Huang, J., Deng, X.J. and Bi, X.Y. (2005). An Extremely Low Visibility Event over the Guangzhou Region: A Case Study. *Atmos. Environ.* 39: 6568–6577.
Wu, D., Bi, X., Deng, X., Li, F., Tan, H., Liao, G. and Huang, J. (2006). Effect of Atmospheric Haze on the Deterioration of Visibility over the Pearl River Delta. *Acta Meteorol. Sin.* 64: 215–223.
Yu, X., Zhu, B., Yin, Y., Yang, J., Li, Y. and Bu, X. (2011). A Comparative Analysis of Aerosol Properties in Dust and Haze-fog Days in a Chinese Urban Region. *Atmos. Res.* 99: 241–247.
Zhang, W., Zhuang, G., Guo, J., Xu, D., Wang, W., Baumgardner, D., Wu, Z. and Yang, W. (2010). Sources of Aerosol as Determined from Elemental Composition and Size Distributions in Beijing, *Atmos. Res.* 95: 197–209.
Zhang, Y. and Li, Z. (2013). Estimation of $PM_{2.5}$ from Fine-mode Aerosol Optical Depth. *J. Remote Sens.* 17: 929–943.
Zieger, P., Fierz-Schmidhauser, R., Poulain, L., Muller, T., Birmili, W., Spindler, G., Wiedensohler, A., Baltensperger, U. and Weingartner, E. (2014). Influence of Water Uptake on the Aerosol Particle Light Scattering Coefficients of the Central European Aerosol. *Tellus Ser. B* 66: 1–14.

Received for review, May 18, 2014
Revised, August 11, 2014
Accepted, October 1, 2014